Depth Profiling by Confocal Raman Microspectroscopy: Semi-empirical Modeling of the Raman Response

J. PABLO TOMBA,* LUIS M. ARZONDO, and JOSÉ M. PASTOR

Institute of Materials Science and Technology (INTEMA), National Research Council (CONICET), University of Mar del Plata, Juan B. Justo 4302, (7600) Mar del Plata, Argentina (J.P.T., L.M.A.); and Department of Physics of Condensed Matter, University of Valladolid, Paseo del Cauce s/n, (47011) Valladolid, España (J.M.P.)

It has been well documented that the use of dry optics in depth profiling by confocal Raman microspectroscopy significantly distorts the laser focal volume, thus negatively affecting the spatial resolution of the measurements. In that case, the resulting in-depth confocal profile is an outcome of several contributions: the broadening of the laser spot due to instrumental factors and diffraction, the spreading of the illuminated region due to refraction of the laser beam at the sample surface, and the influence of the confocal aperture in the collection path of the laser beam. Everall and Batchelder et al. developed simple models that describe the effect of the last two factors, i.e., laser refraction and the diameter of the pinhole aperture, on the confocal profile. In this work, we compare these theoretical predictions with experimental data obtained on a series of well-defined planar interfaces, generated by contact between thin polyethylene (PE) films (35, 53, 75, and 105 μm thickness) and a much thicker poly(methyl methacrylate) (PMMA) piece. We included two refinements in the above-mentioned models: the broadening of the laser spot due to instrumental factors and diffraction and a correction for the overestimation in the decay rate of collection efficiency predicted by Batchelder et al. These refinements were included through a semi-empirical approach, consisting of independently measuring the Raman step-response in the absence of refraction by using a silicon wafer and the actual intensity decay of a thick and transparent polymer film. With these improvements, the model reliably reproduces fine features of the confocal profiles for both PE films and PMMA substrates. The results of this work show that these simple models can not only be used to assist data interpretation, but can also be used to quantitatively predict in-depth confocal profiles in experiments carried out with dry optics.

Index Headings: **Confocal Raman microspectroscopy; Polymer films; Depth resolution; Dry objectives; Refraction.**

INTRODUCTION

Confocal Raman microspectroscopy (CRM) has been widely shown to be a valuable technique for probing chemical/physical properties in sample regions with microscopic dimensions.[1–3] Spatial discrimination is provided by a confocal aperture, designed to collect scattering that originates selectively from the focal plane and to reject contributions from the surroundings. In theory, depth (or axial) resolution in confocal conditions is determined by the diffraction-limited laser focal depth, proportional to the laser wavelength and to the inverse square of the numerical aperture of the objective utilized.[1] For high numerical aperture objectives and the laser wavelengths most commonly used, theory predicts limiting values of depth resolution in the range of 1–2 μm.

One of the most attractive features of CRM is the ability to perform nondestructive in-depth analyses by optical sectioning. In this approach, the laser focus is moved to successively deeper positions in a transparent sample in order to obtain spectral information as a function of depth. Differently from confocal fluorescence microspectroscopy, where the use of water-immersed objectives in biological/medical applications is standard, most Raman microspectrometers are equipped with "dry" metallurgical objectives, where the laser beam is focused at and below the sample surface through air. In that situation, laser refraction at the sample surface has a profound effect on depth resolution. Everall was the first author to point out the misinterpretation of the data that can result when laser refraction is ignored.[4,5] Using a simple model based on geometric optics, Everall modeled and quantified the distortions experienced by the spot illuminated by the laser beam when it was refracted at the air/sample interface, concluding that the illuminated region is spread over a region of tens of micrometers, well beyond the diffraction limit. One of the most striking consequences of his analysis is that depth resolution can be worsened by orders of magnitude compared with the diffraction-limited nominal values, and that deterioration is more severe when one focuses deeper into the sample. It was also shown that the depth scale is artificially compressed, typically by a factor of 2 for a sample with refractive index of 1.5.[4,5]

The pioneering work of Everall has stimulated further contributions and improvements carried out by other authors. For example, Batchelder and co-workers utilized the original framework proposed by Everall to analyze the role of a confocal aperture placed in the collection path of the laser beam.[6] From the results of the model, they concluded that the pinhole effectively contributes to partially block out-of-focus scattering and that although the use of dry optics degrades depth resolution, it is better than what would be expected based only on the axial blurring of the laser beam. A second important prediction of this model is that the collection efficiency decreases dramatically with focusing depth, and this find correlates with the monotonic decrease in Raman signal commonly found in depth-profiling experiments on transparent samples. Bruneel et al. have proposed a simple modification to the model of collection efficiency predicted by Batchelder by introducing an additional term that attempts to describe spherical aberration contributions arising from the off-axis laser intensity distribution.[7]

A different approach to the problem has been recently considered by Sourisseau and co-workers.[8] These authors made use of the rigorous vectorial electromagnetic framework developed by Török et al. for a similar problem.[9] This treatment, possibly the most complete description of the problem, accounts for axial and lateral intensity distributions due to refraction and diffraction and includes the pinhole aperture in the calculations. As a counterpart, the mathematical formulation and the overall strategy to solve the model equations are certainly much more complex than the simple

Received 9 August 2006; accepted 28 November 2006.

* Author to whom correspondence should be sent. E-mail: jptomba@fi.mdp.edu.ar.

0003-7028/07/6102-0177$2.00/0

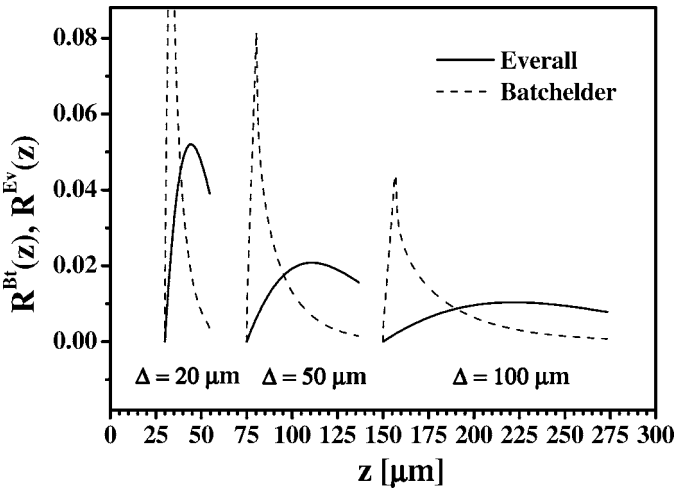

FIG. 1. Depth resolution curves for three values of nominal focusing depth (Δ), as predicted by Everall (solid lines) and Batchelder (dotted lines). All the curves were normalized to unit area. Simulations were carried out with $NA = 0.9$, $n = 1.5$, and $\rho = 1.738$ (equivalent to $\Phi = 500$ μm).

treatments previously described. The model predicts that off-axis refraction and diffraction reduce the axial broadening of the laser, to the extent of reaching fairly constant depth resolution values, independent of the focusing depth.[8] The model also reproduces with remarkable precision the decay in collection efficiency with focusing depth on transparent polymer films.

Many experimental strategies have been suggested to minimize the problem of laser refraction in depth profiling in order to keep depth resolution close to the diffraction-limited nominal values. These strategies include physical sectioning followed by surface analysis or the use of immersion optics with a fluid that matches the refractive index of the sample.[4,5] However, it is not always possible to put them into practice. Obtaining a good micro-cut of cross-sections without disrupting the material requires the use of specific equipment and may be tricky. Being a destructive analysis, it precludes the study of dynamics processes. On the other hand, the use of a fluid in the path of the laser beam may produce spectral overlapping and/or chemical/physical interaction with the sample.

Whenever these strategies are impractical, the use of models to assist data interpretation becomes crucial. A question that remains unanswered is whether the simple and intuitive theoretical analysis by Everall, along with the improvements made by Baldwin and Batchelder, can quantitatively account for the experimentally observed Raman intensity variations with focusing depth, in view of the more complete and sophisticated treatments on the problem that have been recently published.[8] In this work, we try to give a response to this issue. We use as the experimental system a series of carefully designed planar interfaces between polyethylene (PE) films and a thick poly(methyl methacrylate) (PMMA) substrate, which serves as a model for step profiles. The confocal profile of these systems is then compared with model predictions. We consider some modifications of the original treatments, including sources of broadening other than refraction and a correction for the collection efficiency values originally predicted by Baldwin and Batchelder. It will be shown that these simple models reproduce with remarkable precision most of the features observed in depth profiling experiments in the range of depths up to 120 μm.

THEORETICAL

The models of Everall[4,5] and Batchelder[6] use simple ray-tracing analysis to predict the path of the laser beam when it passes through the air/sample interface. In depth profiling, one focuses the laser beam at a nominal point Δ on the z scale, as measured from the air/sample surface according to the scale of the microscope platform. Due to refraction, the infinitesimal laser spot, originally directed at the point Δ, is spread over a range of z values, from z_{min} to z_{max}. According to Everall,[4] z and Δ are related as

$$z = \Delta[m^2 \frac{NA^2(n^2-1)}{1-NA^2} + n^2]^{1/2} \quad (1)$$

where n is the sample refractive index, NA is the numerical aperture of the microscope objective used, and m is the pupil parameter, which varies between 0 for z_{min} (normal incident rays) and 1 for z_{max} (rays with the maximum incident angle). It is considered that the laser intensity has a Gaussian distribution intensity along the pupil lens, $I(m)$, that illuminates the z_{min} to z_{max} region proportionally to the product $m \cdot I(m)$. The Raman response in the axial direction is calculated as

$$R^{Ev}(z) = m^2 \cdot I_0 \cdot \exp(-2m^2) \quad (2)$$

where I_0 is the incident axial intensity. Note that the model ignores the pinhole and neglects orthogonal spreading of the laser beam. Figure 1 shows the collected Raman intensity predicted by Everall for $NA = 0.90$ and $n = 1.5$ (solid lines), as a function of the true focal position (z) for three values of nominal focal positions (Δ). The areas under the curves have been normalized to unity. The results shown in Fig. 1 illustrate the effect of laser refraction on depth resolution and constitute the essence of the analysis of Everall: Raman scattering is collected over an increasingly wider region that lies much deeper than the nominal point where the laser beam was originally focused (Δ), and these regions are extended over distances on the order of tens of micrometers, much larger than the diffraction-limited depth of focus.

Baldwin and Batchelder[6] refined the treatment of Everall by considering that in the collection path the confocal system blocks some of the refracted rays, restricting the fraction of illuminated region from which Raman scattering is primarily detected. The authors modeled the effect of the air/sample interface on the collection aperture of the confocal system and calculated, for each axial illuminated spot, how much of the Raman scattered light is allowed to pass by a confocal back aperture of radius ρ. Following Batchelder, the collected Raman intensity is calculated as

$$R^{Bt}(z) = m \cdot I_0 \cdot \exp(-2m^2) \cdot \Omega(\Delta, n, NA, \rho) \quad (3)$$

where Ω, the collection solid angle, measures the efficiency of the confocal system. The equations and numerical methods used to calculate $\Omega(\Delta, n, NA, \rho)$ can be found in Ref. 6.

Before introducing the predictions of the model of Batchelder, we briefly explain the way in which the pinhole aperture is related to the radius of the virtual image of the confocal aperture in the focal plane (ρ), as defined in the model of Batchelder. In the LabRam instrument, the pinhole is squared and the value one sets in the software corresponds to the diagonal of the square expressed in μm (Φ). The magnification between the sample and the confocal hole is

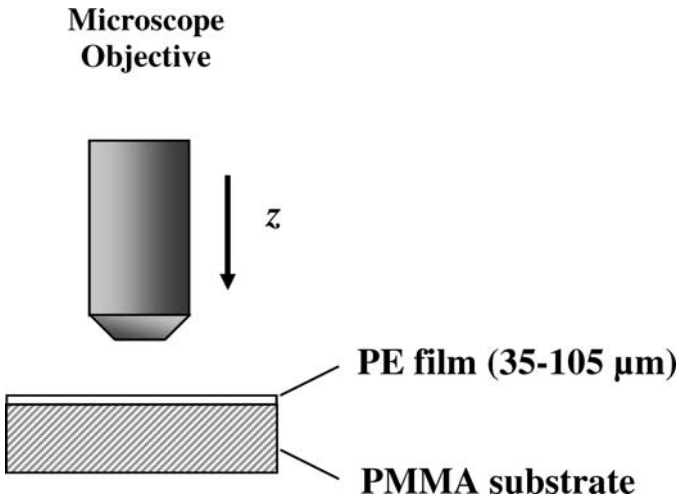

FIG. 2. Scheme of the experimental configuration used. The laser beam is focused along the z-axis, through air, at successively deeper positions into the sample.

the microscope magnification (M) multiplied by a factor of 1.4.[10] For example, a hole of 280 μm used with a 100× objective corresponds to a sampled area of 2 μm. Thus, Φ is approximately related to ρ as $\Phi = 1.4 \cdot M \cdot 2\rho$. The predictions of the model of Batchelder are shown in Fig. 1 with dotted lines, for values of $NA = 0.9$, $n = 1.5$, and $\rho = 1.786$ (equivalent to $\Phi = 500$ μm). Although in the original treatment by Batchelder the area under the depth-resolution curve reflects the collection efficiency of the pinhole at a given Δ value, we normalized the areas under the curves to unity for easier comparison. The peaked shape of the $\Omega(z)$ curves[6] concentrates the sampled region into a smaller volume than that predicted in the absence of a pinhole, yielding a sharper overall response with depth compared with Everall's predictions.

Raman responses to planar interfaces are calculated by convoluting the theoretically expected step profiles $R^{St}(z)$ with the depth response curves predicted by Everall or Batchelder, $R^{Ev,Bt}(\Delta, z)$:

$$I^{Ap}(\Delta) = \int_{z_{min}}^{z_{max}} R^{St}(z) R^{Ev,Bt}(\Delta, z) dz \qquad (4)$$

So far, we have only considered distortions by refraction originated from a laser beam that in the absence of refraction would illuminate a sample spot of infinitesimal dimensions. In a more realistic situation, the laser spot originally has an intensity distribution along the optical axis of the microscope due to other sources of broadening such as diffraction and/or instrumental factors, which is further refracted. The term "instrumental factors" refers to any broadening source other than diffraction, for instance, those associated with the mismatch of the apertures of the coupling optics along the light path. This contribution, here referred to as $R^{Df}(z)$, is assumed to be known for a given set of instrumental conditions and to be invariant with focusing depth. The response of a step profile broadened by diffraction/instrumental factors $I^{St\text{-}Df}(z)$ is thus calculated by the following convolution integral:

$$I^{St-Df}(z) = \int_0^\infty R^{St}(z') R^{Df}(z' - z) dz' \qquad (5)$$

Finally, apparent depth profiles distorted by diffraction plus refraction are calculated as a function of Δ by convoluting the response of the step profiles distorted by diffraction/instrumental factors with the depth resolution function due to the refraction $R(z_m)$, as calculated from the models of Everall or Batchelder:

$$I^{Ap}(\Delta) = \int_0^\infty I^{St-Df}(z) R^{Ev,Bt}(z, \Delta) dz \qquad (6)$$

EXPERIMENTAL

The polymers used in this work, polyethylene (PE) and poly(methyl methacrylate) (PMMA), have similar refractive indexes, 1.51 and 1.49, respectively. PE films with thicknesses in the range 20–200 μm are commercially available. For these experiments we used PE films with four different thicknesses: 35, 53, 75, and 105 μm. Film thicknesses were measured with a Mitutoyo micrometer (model 395–271), with ±1 μm precision. The PMMA piece used as substrate (several millimeters thick) was vacuum-molded and then carefully polished.

Planar PE/PMMA interfaces were generated simply by putting the flexible PE film in contact with the PMMA piece, as shown in Fig. 2. Neither thermal treatment nor adhesives were used to promote contact between the polymers; in this way, any distortion on the shape of the planar interface was avoided. The PE film was maintained in position using holders, adjusted to apply a slight tensile force on the edges of the film. The PMMA piece has a smooth convex curvature on the top, which, combined with the tensile force applied to the film borders, produces a good contact between film and substrate.

Raman spectra were recorded at room temperature, on a Raman microspectrometer DILOR LabRam Confocal, equipped with a 16 mW HeNe laser beam (632.8 nm wavelength). A slit opening of 500 μm and a holographic grating of 1800 lines/mm were used, rendering a spectral resolution of 5 cm^{-1}. We used a dry Olympus 100× objective ($NA = 0.9$, 210 μm working distance) in combination with variable pinhole openings (the maximum aperture is 1000 μm). For depth profiling, the samples were mounted on a microscope stage with vertical displacement (z-axis) controlled manually with the micrometric screw of the microscope. Raman intensity depth profiles were measured by taking Raman spectra from different depths, moving the stage vertically (z) in steps of 2 μm.

Polyethylene and PMMA have characteristic Raman spectra, as shown in Fig. 3 for the range of Raman shifts 1000–2000 cm^{-1}. An example of a composite spectrum, i.e., that obtained in the proximities of the PE/PMMA interface, where both components contribute to the Raman signal, is also shown in that figure (bottom curve). To individually compute the Raman intensity of the PE and PMMA components, we applied the linear decomposition method.[11] The technique reconstructs the composite spectrum through a linear expansion in terms of the spectra of the individual components. For the calculations, the method employs the whole Raman profile, i.e., Raman intensities in the 1000–2000 cm^{-1} spectral range, instead of the intensity of a single band. The weight coefficients of the linear expansion directly measure the relative contribution of individual components to the global spectrum.[11] This information is plotted versus the focusing depth in order to obtain the corresponding in-depth confocal profile.

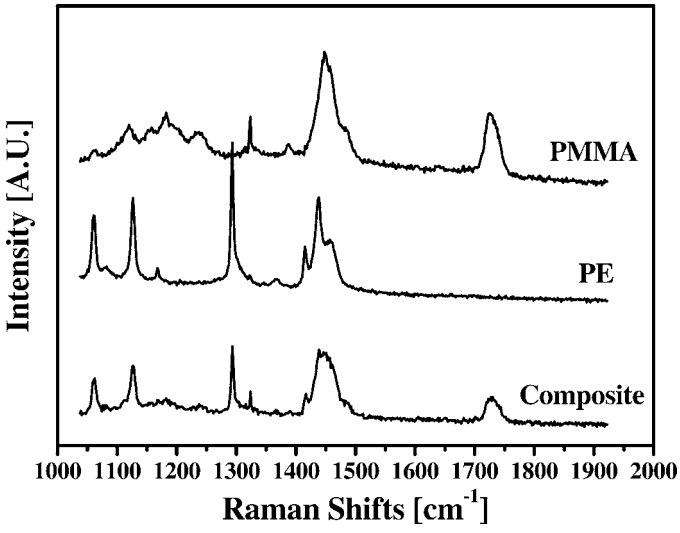

FIG. 3. Raman spectra of the pure components (PE and PMMA) along with a composite spectrum that reflects both contributions.

RESULTS AND DISCUSSION

Raw Raman Depth-Profiles for Planar Interfaces. Figures 4A through 4C show the Raman intensity profiles obtained from in-depth studies on the series of planar PE/PMMA interfaces scanned through air with a 100× metallurgical objective (*NA* = 0.9). Figure 4A shows the Raman response of the PE films, while Fig. 4B shows the corresponding Raman response of the PMMA piece (several millimeters thick), as measured through the PE film. These data were acquired with a confocal aperture of 500 μm. Figure 4C shows the Raman responses of PE films (35 and 55 μm thick) for other pinhole apertures (200 and 800 μm). Raman intensities were calculated from the relative contributions of individual components to the global spectrum, as obtained after applying the linear decomposition method.[11] Note that all the Raman intensity profiles shown in Fig. 4 were normalized with respect to its maximum value. The depth scale corresponds to the nominal focusing depth (Δ) as determined from the micrometric screw of the microscope, where zero corresponds to the PE film's outer surface.

We scanned the interface, focusing the microscope 20 μm above the PE film surface, and then moving the focal point in the sample direction. For this reason, Raman intensity starts from a value near zero, when the focal volume is in air, and rapidly increases when it passes through the sample surface and finally reaches the sample (see Fig. 4A). The intensity profiles present the typical features of depth-profiling experiments with dry objectives: the planar interfaces appear significantly broadened and apparently located at lower depths than those expected on the base of the nominal thicknesses of the PE films. As a measure of the apparent position of the planar interface, we used the maximum of the derivative curve of the PE intensity profile. The analysis yields values of apparent location of 19, 32, 44, and 62 μm. Compared with the nominal thicknesses of the PE films (35, 53, 75, and 105 μm), we conclude that the depth scale appears artificially compressed by a factor of about 1.7. Both effects, the apparent compression in the depth scale and the artificial broadening of the planar interface, are consequences of the laser refraction at the air/sample interface, as well documented by Everall.[4] Another

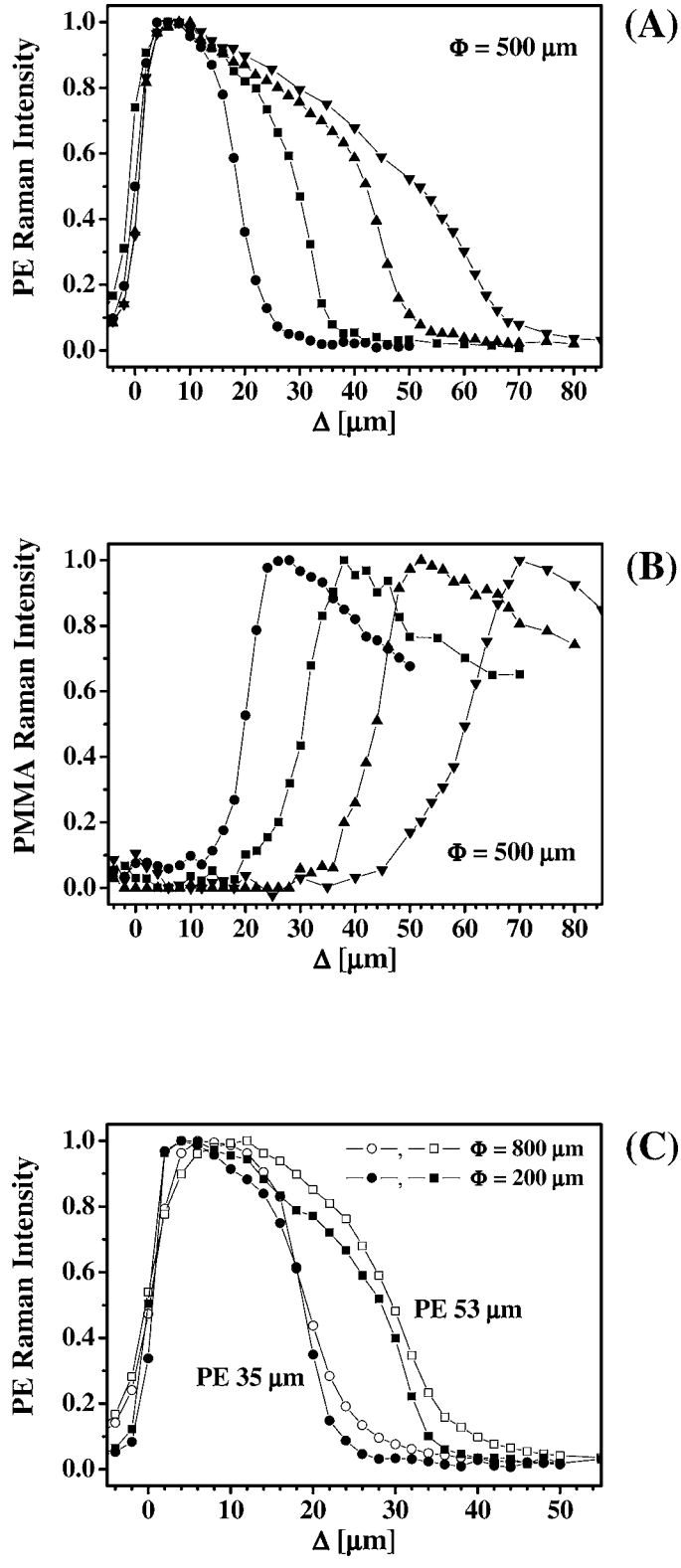

FIG. 4. Experimental Raman in-depth intensity profiles. (**A**) PE films with thicknesses of 35 μm (circles), 53 μm (squares), 75 μm (up triangles), and 105 μm (down triangles), measured with Φ = 500 μm; (**B**) PMMA thick substrate as measured through the PE films with the same pinhole aperture; (**C**) PE films with thicknesses of 35 μm (circles) and 53 μm (squares), measured with Φ = 200 and 800 μm. All the experiments were carried out with a 100× dry objective (*NA* = 0.9).

characteristic feature of the experiments is the asymptotic Raman response as the focal point moves away from the planar interface. It is well observed in the PE response ahead of the transition region that asymptotically approaches zero in the form of an extended tail. The same is observed in the PMMA response, where a large tail precedes the sudden increase in Raman intensity when the focal volume passes through the PE/PMMA interface. We will see later that these tails are not predicted by the models that only account for refraction, and that it is necessary to include other corrections to properly predict the observed response.

Another typical feature of depth-profiling experiments is the fall in the collected Raman signal with focusing depth. This effect is easily seen in Fig. 4A for the thicker PE films as a progressive decrease in Raman intensity throughout the material. The same effect is observed in Fig. 4B as a fall in the Raman response when the actual focal volume is mostly within the PMMA layer. The model developed by Baldwin and Batchelder very simply predicts this effect, also attributed to laser refraction. Note that the decay in the collected Raman intensity with focusing depth is not predicted by Everall's model, as his treatment does not consider the presence of the pinhole. Although this is not the case here, sample absorption or scattering effects may also affect the collected Raman intensity with focusing depth, particularly in nontransparent samples.[12]

Figure 4C illustrates the effect of the pinhole aperture on the Raman intensity profiles. The example shows the response of PE films with thicknesses of 35 and 53 μm, as obtained with markedly different pinhole apertures (200 and 800 μm). The pinhole aperture mainly affects the size and extension of the tails of Raman intensity when the apparent focus position passes from the air to the sample and through the PE/PMMA interface. However, the apparent thickness of the PE film and the breadth of the PE/PMMA transition are not much affected. In this experimental configuration, reducing the pinhole opening does not substantially enhance depth resolution as refraction aberrations overwhelm the improvement in axial resolution that could be expected in confocal conditions. In this way, the main effect of the confocal aperture is to determine the overall collected intensity. Notice that the rate of decay of Raman intensity throughout the PE film shows a minimal dependence on the size of the pinhole aperture.

Modeling of the Raman Response. The convolution integrals given by Eqs. 4–6 allow us to calculate the Raman response of planar interfaces distorted by refraction and/or diffraction/instrumental factors for a given set of experimental conditions, i.e., *NA*, *n* and Φ. Figure 5 shows different aspects of the simulated Raman response of a planar interface between a 75 μm PE film and a much thicker PMMA layer. We start by considering the simplest situation, the case of pure refraction, as predicted by Everall (dotted lines) and Batchelder (dashed lines) in Figs. 5A and 5B. Figure 5A corresponds to the Raman response of the PE film, while Fig. 5B shows the PMMA layer intensity profile, as measured through the PE film. The zero in the depth scale corresponds to the air/PE interface. The simulated results were obtained by solving Eq. 4 with a step profile representing a planar PE/PMMA interface located 75 μm from the outer PE surface. We assumed a homogeneous medium with $n = 1.51$ along with $NA = 0.9$ and $\Phi = 500$ μm.

The model of Everall predicts some of the features found in the experiments (compare with Fig. 4A): (1) the PE layer, 75

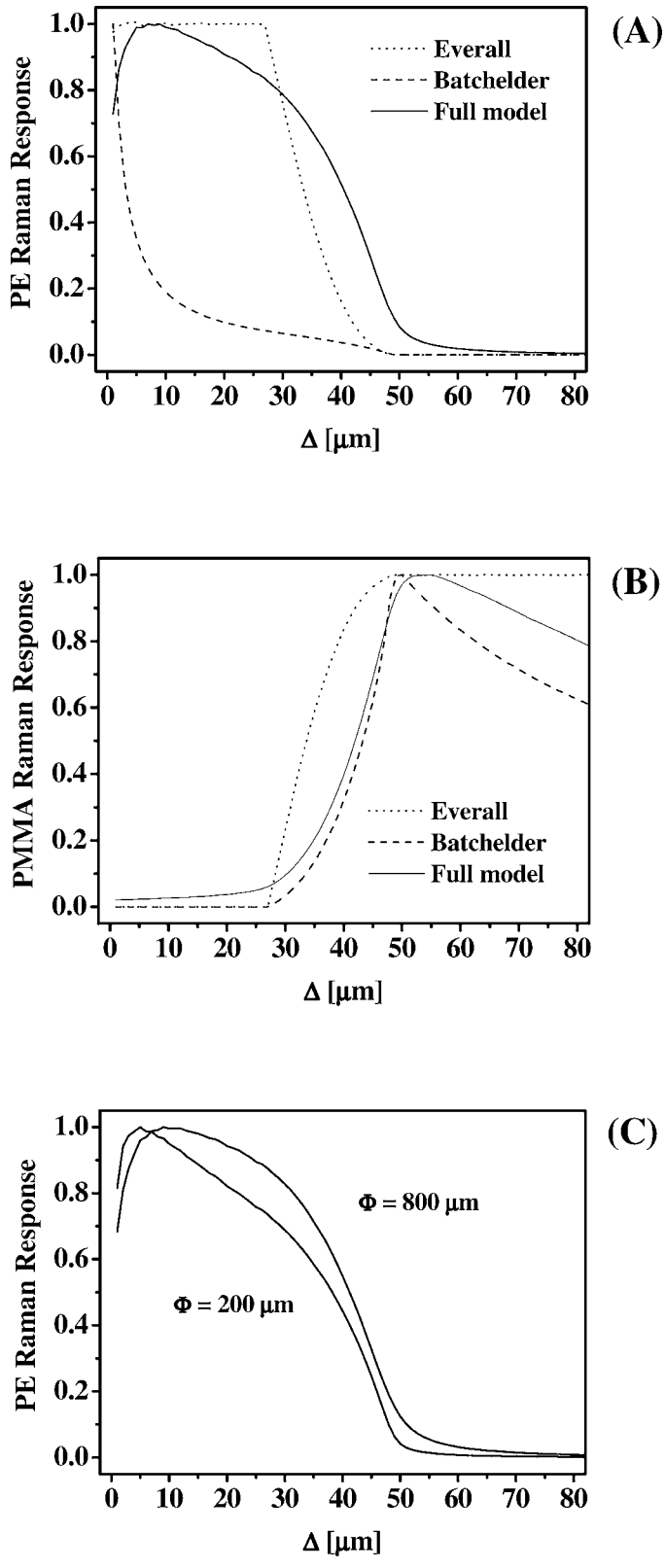

FIG. 5. Simulated confocal Raman response as a function of the nominal focusing depth for a planar interface composed of a 75 μm thick PE film and a thick PMMA piece. Simulations correspond to $NA = 0.9$ and $n = 1.51$. (**A**) PE response ($\Phi = 500$ μm); (**B**) PMMA response ($\Phi = 500$ μm); (**C**) PE response for two different pinhole apertures.

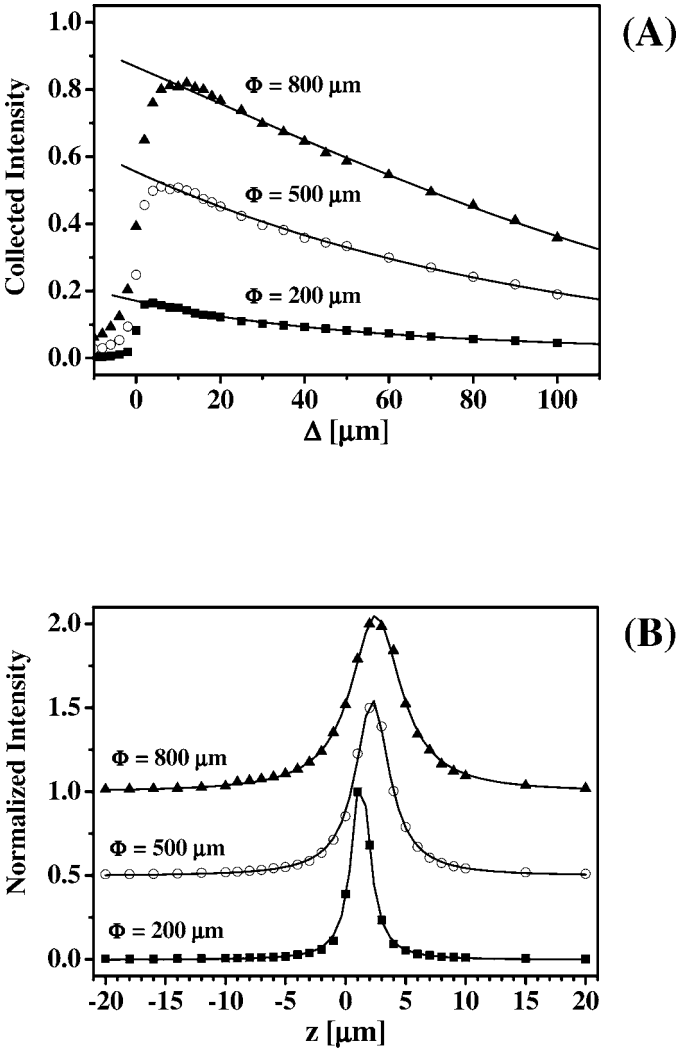

FIG. 6. (**A**) Raman intensity profiles of a thick transparent sample (PE) for three different pinhole apertures. The solid lines correspond to the fittings used in computational simulations. Fitting function: $\log I(\Delta) = a + b\Delta + c\Delta^2$; fitting parameters [$a$; b; c]: $\Phi = 200$ [-0.77; -7.2×10^{-3}; 1.5×10^{-5}]; $\Phi = 500$ [-0.26; -4.5×10^{-3}; -8.1×10^{-7}]; $\Phi = 800$ [-6.2×10^{-2}; -2.7×10^{-3}; -1.1×10^{-5}]. (**B**) Raman intensity profiles of a silicon wafer scanned in the z direction for three Φ values. Lorenztian fittings are indicated with solid lines.

μm thick, appears artificially thinned, by a factor of about two; (2) the interlayer transition, expected to be very sharp, is extended over a quite broad region. However, the model does not account for the fall in Raman intensity with focusing and overestimates the apparent compression in the depth scale.[5,13,14] These issues are partially solved with the improvements introduced by Baldwin and Batchelder through the function $\Omega(z)$, which essentially shifts the collection volume at larger depths (see Fig. 1) and predicts a monotonic decrease in Raman signal with focusing depth.[6] Although the model predicts quite well the resulting improvement in depth resolution associated with the presence of the pinhole aperture, it largely overestimates the fall rate of the Raman intensity with focusing depth. This discrepancy was first reported in Ref. 13 and the results found here confirm the disagreement between model predictions and experimental data. Figure 5A makes evident this issue, where one sees that the model predicts a much faster fall in Raman intensity than that observed in the experimental data. Figure 5B shows that the predicted response for the PMMA layer is close to the trend observed in the experimental data (compare with Fig. 4B). In this case, the lack of precision in predicting the fall rate in Raman intensity is counterbalanced by the sudden increase in Raman intensity that occurs when the focal volume passes through the PE/PMMA interface. Compared with the calculations of Everall, the model of Batchelder predicts an apparent position for the interface shifted at larger depths (about 10 μm), in agreement with the depth resolution curves already shown in Fig. 1. Other features of the experimental data, such as the asymptotic Raman response observed as the focal point moves away from the interface, are not predicted by the models considered here. Instead, the models predict sharp transitions where the Raman signal converges very rapidly to zero.

With the aim of obtaining a better matching with the experimental data, we considered a series of refinements in the scheme proposed by Everall and Batchelder. First, we corrected the overestimation in the intensity fall rate predicted by the model of Batchelder. In this case, we followed an empirical approach based on independent measurements on thick films.[13] In these experiments we simply tracked the collected Raman intensity as a function of the apparent focusing depth on a thick film (500 μm) made of the same PE grade. Figure 6A shows experimental data (symbols) corresponding to three different pinhole apertures (200, 500, and 800 μm). As the PE sample studied is transparent, the decay curve should only reflect the effect of the pinhole on the collection efficiency, as described by Batchelder. Indeed, other transparent samples examined (e.g., polystyrene, PMMA) exhibited the same decay rate. However, some other thick polyethylene samples of different grade, visually opaque, exhibited higher fall rates. It certainly indicates that other factors, i.e., diffuse reflectance or scattering, may also contribute to intensity losses. The complex phenomena associated with the variations of collected Raman intensity with focusing depth raise the issue of correctly predicting those variations based only on models that consider the transmitted flux through the pinhole aperture.[6,14] In the best of the cases, these models are only applicable to transparent samples.

To correctly predict the intensity profiles of the PE/PMMA interfaces we use the experimentally measured decay rate of the PE film as a factor to renormalize the area under the depth resolution curves predicted by Batchelder in Fig. 1. The experimental decays were first fitted to exponential functions, i.e., $\log I(\Delta) = a + b\Delta + c\Delta^2$, as shown in Fig. 6A with solid lines. In the choice of the form of this equation, we privileged a good fitting to the data, even sacrificing physical meaning; for a sounder approach, see the equation proposed in Ref. 7. We found that the experimental decay rates were slightly dependent on the pinhole aperture; therefore, we used different fitting parameters for each Φ value, as reported in the caption of Fig. 6. Briefly, the correction consists of multiplying each curve of depth resolution for a given value of nominal depth, by the experimentally observed Raman intensity at this point, as determined from the corresponding fitting curve. Then, this family of corrected curves is used to calculate the convolution integrals.

A second improvement in the model is the incorporation of broadening sources other than refraction, i.e., diffraction/instrumental factors. We account for these effects through the function $R^{\mathrm{Df}}(z)$ in Eq. 5. To correctly characterize this

contribution, we have again sought for a semi-empirical approach, consisting of measuring the Raman step-response in the absence of refraction. A reliable and simple experiment that provides this information consists of scanning a silicon wafer in the z-direction. As the laser beam does not penetrate significantly into silicon, the wafer surface behaves essentially like a layer of infinitesimal thickness and the experiment provides a point-by-point measure of the broadening in the absence of refraction. Raman profiles of this experiment are shown in Fig. 6B (symbols) for three different pinhole apertures, where the y-axis corresponds to the intensity of the silicon line at 520 cm^{-1}. The full-width at half-maximum (FWHM) of these curves, 1.95, 3.5, and 5.2 μm, represent the depth resolution in the absence of refraction. The silicon intensity profiles were fitted to Lorentzian functions (solid lines), which were used as $R^{Df}(z)$ in Eqs. 5 and 6 assuming invariance in shape with focusing depth.[1,15]

We show examples of such corrections in Figs. 5A and 5B (solid lines) for a pinhole aperture of 500 μm. With these improvements, finer features of the experimental data are now better reproduced. For example, the increase in Raman intensity while the focal volume passes from air to the sample, followed by a much slower fall throughout the PE film than that predicted by Batchelder, gives an overall shape that looks very similar to that observed in the experimental data, as seen in Fig. 5A. The position of the apparent interface is shifted at larger depths compared with Everall's prediction. Similar conclusions can be drawn from Fig. 5B. Extended tails, ahead of the PE/PMMA interface in the PE response and preceding the sudden increase in the PMMA response, are now predicted as a consequence of the combined effects of diffraction/instrumental broadening and refraction. Figure 5C shows the predicted response for two different pinhole openings, and we see that the simulations reproduce very well the overall shape observed in the experimental data (compare with Fig. 4C). The next section develops a direct comparison between computational results and experimental data.

Comparison Between Model Predictions and Experiments. In Fig. 7 we compare model predictions (solid lines) with experimental data (symbols) for the series of PE/PMMA planar interfaces examined. Figures 7A through 7D show the response of the thin PE films (open symbols) along with the response of the thick PMMA layer (solid symbols), as measured through the PE film, for PE thicknesses of 35 μm (Fig. 7A), 53 μm (Fig. 7B), 75 μm (Fig. 7C), and 105 μm (Fig. 7D) and for a pinhole aperture of 500 μm. Figures 7E and 7F compare the Raman intensity profiles obtained with other pinhole apertures (200 μm in Fig. 7E, and 800 μm in Fig. 7F).

To carry out the simulations, we assumed a homogeneous medium with $n = 1.51$ and $NA = 0.9$. To define the step function $R^{St}(z')$ in Eq. 5, we used the nominal thickness values of the PE films, as determined from independent measurements (see the Experimental section). The silicon profile and the decay in Raman intensity (Fig. 6) were chosen accordingly with the pinhole aperture utilized in the experiment. Through these figures we see that the predicted Raman response is very close to that measured for both PE films and the PMMA layer. The decay rate of the Raman intensity throughout the PE film, the apparent position of the interface, and its broadness are very well reproduced for all the systems studied. The large tails ahead of the PE response and preceding the sudden increase in the PMMA signal are now well accounted for by the simulations. Notice that the position of the interface in the step function was considered as a fixed parameter, equal to the nominal value of the PE film thickness, and that the matching with the experimental data could have possibly been improved by setting the interface position as a fitting parameter. In any case, the agreement between model predictions and experimental data is remarkable given the wide range of thicknesses and pinhole apertures tested and is comparable to that obtained using more sophisticated approaches. In fact, some fine features of the intensity profiles, such as the asymptotic Raman response, are better reproduced here; see, for example, Fig. 3 of Ref. 14 or Fig. 7 of Ref. 8, works in which diffraction is accounted for theoretically but other sources of broadening are disregarded.

Although the good matching with the experimental data is encouraging, some issues, such as the way the model accounts for the pinhole aperture, require attention. The fact that the model of Batchelder largely overestimates the fall rate in Raman intensity with focusing depth indicates deficiencies in the model, as cleverly pointed out by Bruneel et al. in a recent work.[7] One of the reviewers suggested that the use of a simple lens in the model may be a factor to consider; this suggestion definitively makes sense, bearing in mind that more complete and precise treatments include, among other refinements, spherical aberration effects.[7,8] In any case, the development of a model that accounts completely and effectively for all these features is a difficult task given the complexity and particular details of the optical configuration of each instrument. On the other hand, the fact that the model well predicts the effective depth of focus and consequently the apparent position of the planar interface certainly indicates that other effects, not accounted for here, such as off-axis contributions, may effectively operate to further improve depth resolution.[8] Other alternatives have been recently proposed to account for the effect of the pinhole aperture on depth resolution, based on simple expressions for the flux transmitted through the circular aperture.[14] These treatments are analogous to that considered here, in the sense that the function that describes variations in the transmitted flux with the focal point essentially shift the Raman response at larger depths, predicting a sharper depth resolution. However, these models have been criticized for some rather arbitrary assumptions employed in their formulation; for a detailed discussion see Ref. 8.

We end the paper with a comment about the actual values of spatial resolution in depth-profiling experiments. In recent works, it has been suggested that diffraction and off-axis intensity distributions may operate to reduce the axial spreading of the laser focus, to the extent of reaching fairly constant depth resolution values, on the order of 5–6 μm, independently of the focusing depth.[7,8,16,17] The results of these experiments show that this may not be the case. A visual examination of the results shown in Fig. 4 shows that the breadth of the apparent interface increases with the thickness of the PE film, i.e., with the location of the interface measured from the PE surface. The extent of this artificial broadening can be quantified from the derivative curves of the corresponding profiles (not shown here). For example, the resulting bell-shaped derivative curves obtained from the PE signal at $\Phi =$ 500 μm yielded FWHM values of 7.4, 8.3, 9.3, and 15.0 μm for planar interfaces nominally located at 35, 53, 75, and 105 μm. These results indicate that depth resolution does degrade with focusing depth, as originally predicted by Everall. Notice that

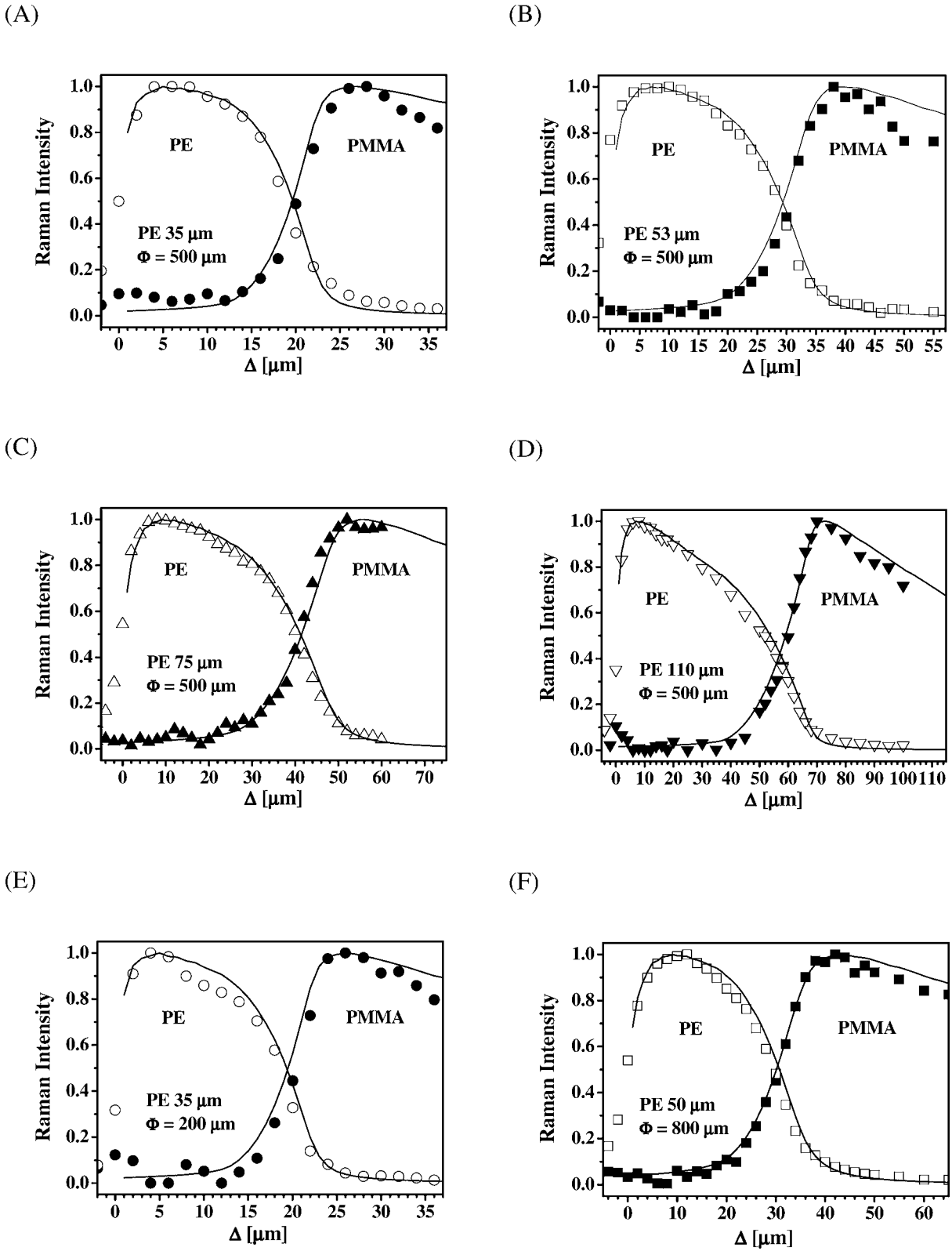

FIG. 7. Confocal profiles of planar interfaces for the systems studied. The symbols correspond to data measured with dry optics for the experimental conditions indicated in the plot. The full lines represent computational results.

all these FWHM values were calculated based on the scale of apparent focusing depth (Δ), artificially compressed by a factor between 1.5 and 2, which means that the actual values of depth resolution are expected to be additionally worsened by this factor. A similar conclusion was inferred by Bruneel, after examining the response of a silicon wafer through variable thicknesses of oil, although the authors observed that for lower NA objectives (0.75), depth resolution reaches a limiting value

of about 13 μm when focusing depths were larger than 300 μm.[7]

CONCLUSION

This work has shown an extensive comparison between predictions of simple models for depth resolution and experimental data in dry-optics CRM experiments. Although the original treatments of Everall and Baldwin and Batchelder nicely capture some of the features of the intensity profile with a minimum set of inputs (n, NA, Φ), it was necessary to include further refinements to reproduce fine details of the observed response. The corrections proposed, i.e., the inclusion of the on-axis intensity distribution of the laser spot in the calculations and the renormalization of the depth-resolution curves with values of collection efficiency obtained from independent experiments, significantly improved the matching between experimental data and model predictions. We showed, for the first time, that these models quantitatively reproduce the confocal profiles of both the thin film and the thicker substrate for a wide range of film thicknesses and using different confocal apertures. However, some issues, such as the way in which the pinhole affects the collection efficiency in this simple framework, require a more detailed analysis. In any case, and given the difficulties in performing detailed modeling of the complex and particular features of the optics of each instrument, a semi-empirical approach to the problem, where instrumental sources of broadening can be reliably characterized by means of independent experiments, appears as a wise alternative.

ACKNOWLEDGMENTS

This project was funded by CONICET (PIP No. 6251). J. P. Tomba would like to thank Drs. L. Izaguirre and M. Herguedas for their valuable assistance during CRM measurements.

1. R. Tabaksblat, R. J. Meier, and B. J. Kipp, Appl. Spectrosc. **46,** 60 (1992).
2. G. J. Puppels, F. F. M. de Mul, C. Otto, J. Greve, M. Robert-Nicoud, D. J. Arndt-Jovin, and T. M. Jovin, Nature (London) **347,** 301 (1990).
3. G. P. Puppels, W. Colier, J. H. F. Olminkhof, C. Otto, F. F. M. de Mul, and J. Greeve, J. Raman Spectrosc. **22,** 217 (1991).
4. N. Everall, Appl. Spectrosc. **54,** 773 (2000).
5. N. Everall, Appl. Spectrosc. **54,** 1515 (2000).
6. K. J. Baldwin and D. N. Batchelder, Appl. Spectrosc. **55,** 517 (2001).
7. J. L. Bruneel, J. C. Lassegues, and C. Sourisseau, J. Raman Spectrosc. **33,** 815 (2002).
8. C. Sourisseau and P. Maraval, Appl. Spectrosc. **50,** 558 (1996).
9. P. Török, P. Varga, and G. Németh, J. Opt. Soc. Am. A **12,** 2660 (1995).
10. *LabRam Manual* (Jobin Yvon-HORIBA, France, 1995).
11. J. P. Tomba, E. de la Puente, and J. M. Pastor, J. Polym. Sci., Part B: Polym. Phys. **38,** 1013 (2000).
12. S. Hajatdoost and J. Yarwood, Appl. Spectrosc. **57,** 1324 (2003).
13. J. P. Tomba and J. M. Pastor, Vib. Spectrosc., paper submitted (2006).
14. L. Baia, K. Gigant, U. Posset, R. Petry, G. Schottner, W. Kiefer, and J. Popp, Vib. Spectrosc. **29,** 245 (2002).
15. J. Vyorykka, J. Paaso, M. Tenhunen, H. Iitti, T. Vuorinen, and P. Stenius, Appl. Spectrosc. **57,** 1123 (2003).
16. N. Everall, Spectroscopy **19,** 16 (2004).
17. N. Everall, Spectroscopy **19,** 22 (2004).